Stability limit state design of box sections supporting mining and process facilities

Osama Bedair*

Technip Corporation, 116 Mt. Aberdeen Manor SE, Calgary, Alberta, T2Z 3N8, Canada

Abstract.   The design of box girders requires the determinations the buckling stress of the flange and the webs. Existing design equations available in codes of practice ignore the interactions between the box girder components. The paper illustrates the influence of the geometric interaction on the buckling stress of box girders. Generalized equations are first derived in terms of the web the flange geometric properties. Industrial examples are then presented showing the variation of the flange buckling stress for various stiffening configurations. The influence of the flange/web proportions on the buckling stress of box girder components is also highlighted. It is shown that buckling strength of the flange is largely affected by the restraints imposed by the webs or attached diaphragms. Graphs are presented showing various limiting states of box girders. These graphs are useful to use in practice in order to achieve economical and efficient design of box girders and rationally predict local buckling stress.

Keywords: steel design; structural analysis; industrial facilities

1. Introduction

Box girders are extensively used in bridge constructions and are also used to support mining and process facilities. As an example, the surge facility shown in Fig. 1, used in the material handling unit is supported by series of longitudinal girders. The average weight of the surge facility is approximately 2,600 tons. The box girder supports are normally designed to accommodate heavy loads caused by dumping and storage of the oil-sands. The structure consists of; 1) a hooper with horizontal leaf gates; 2) spillage conveyor; 3) apron feeders; 4) mix box feed conveyor; 5) electrical house and mechanical equipments; 6) air blasting and HVAC systems. During operation, oil sand material is placed in the hopper by a surge feed conveyor, then it is dumped into the apron feeders, and then discharged by the chute into the mix box feeder conveyor. Paddle shafts are mounted above the drives of the apron feeders in order to minimize congestion during operation. The spillage conveyor collects the material spilled by the apron feeder and dumps it into the discharge chute.

It is common in practice to stiffen the flanges and the webs in the longitudinal and transverse directions to enhance the structural stability during operation. The profile of the ribs (or stiffeners) may also vary in practice. Open stiffening ribs are usually flat bars, inverted tees (or WT section), angles, *L*, or bulb sections. Although closed ribs have considerable torsional rigidity, their

*Corresponding author, Ph.D., E-mail: obedair@gmail.com

Fig. 1 Surge bin facility supported by box girders

fabrication is more difficult than open ribs. Due to the high loads induced during operation, several failure modes may result. Some of there failures are caused by the geometric interaction between the box girder components which is ignored by current design codes of practice. Objective of the paper is to highlight the influence of the geometric restraints restraints on the computation of the buckling stresses.

Several investigations were done in the past for analysis of stiffened panels used for various engineering applications. Rikards *et al.* (2001) used Finite Element for analysis of stiffened plates. They used magnified stiffness values at the plate/stiffener points of contacts. Barik and Mukhopadhyay (2002) presented FE formulations for analysis of plates with arbitrary geometrical configurations. Patel *et al.* (2006) used FE formulations for analysis of stiffened panels subjected to uniform in-plane harmonic edge loading. Mallela and Upadhyay (2006) used ANSYS to present parametric study on simply supported laminated composite blade-stiffened panels subjected to in-plane shear loading. Zhang *et al.* (2005) presented finite element formulation for analysis of stiffened plates under heavy fluid loading. They incorporated in their formulations the radiation damping effect due to the fluid loading. Stamatelos *et al.* (2011) presented a methodology to study local buckling and post-buckling behavior of stiffened plates. Transverse and rotational springs of varying stiffness were used to model the plat-stiffener interaction. A two-dimensional Ritz displacement function is utilized in the analysis. Zhang *et al.* (2011) used a triangular composite stiffened plate/shell element to analyze stiffened plates using Mindlin shear deformation theory. The rotations of ribs and the plate are determined using displacement compatibility conditions. Tamijani and Kapania (2010) investigated stability of plates with curvilinear stiffeners subjected to in-plane loading. The transverse deflection and rotations of the plate and stiffener were expressed in terms of Chebyshev polynomials. The stiffness and geometric stiffness matrices are obtained by superimposing the strain energy and potential of the membrane force in curvilinear coordinates. Li and Xiaohui (2010) presented finite element model to study the bending behavior of stiffened plates. The compatibility of displacements and stresses between the plate and the stiffeners conditions were used to establish the governing equations. Nath (2010) presented analytical solutions for elastic fields of a stiffened plate subjected to axial tension and pure bending. A potential function is
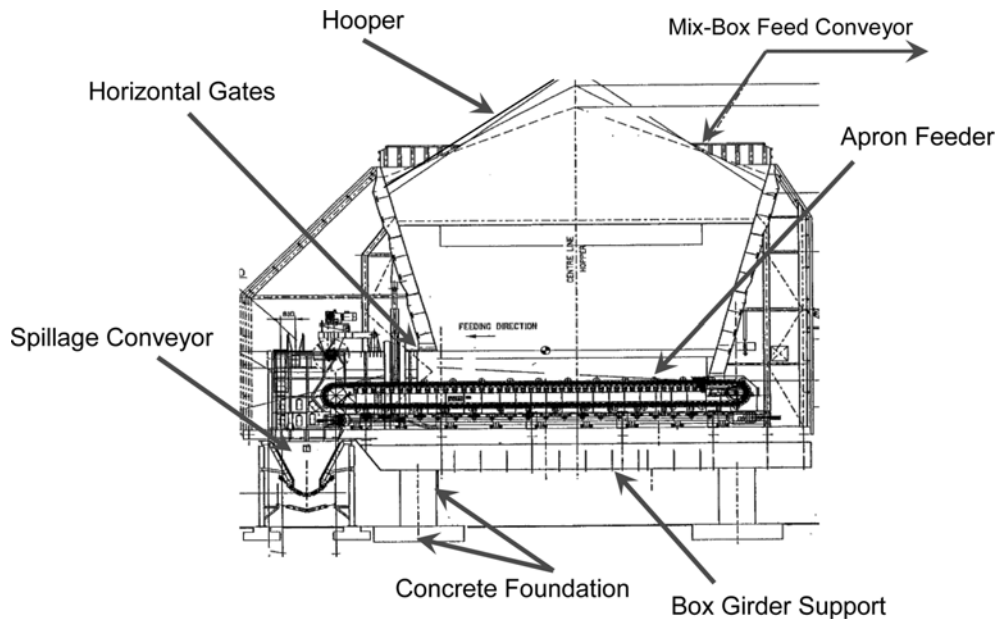
Fig. 2 Section elevation showing structural components of the surge bin facility

expressed in terms of the displacement components that satisfy the equilibrium condition. Fourier series approximation is then used to satisfy the boundary conditions. It must be highlighted that the Finite element and finite strip methods requires extensive computer storage, cost and data preparation from the user if the stiffeners are not equally spaced or have different profiles, or the applied load is not uniform as in the case of the many of the oil-sand facilities.

The above studies dealt with specific aspects that affect the design of box girders. Limited literature addressed the stability of box girders with applications to industrial facilities. It was found during several industrial investigations that the geometric interactions are very critical and may yield unpredicted failures. Objective of the paper is to study the influence of the web/flange geometric interaction on the stability of box girders with application to mining process facilities.

2. Numerical model

Consider typical box girder support shown in Fig. 3, with flange width (b_f) and thickness (t_f). The width of the web is denoted by (b_w) the thickness by (t_w). Section A-A is showing the box girder profile with longitudinal ribs. Section B-B shows typical transverse rib profile. The superscripts L and T are used to denote the longitudinal and transverse rib, respectively. Each rib is described by the following geometric properties; A = cross-sectional area, Q = first moment of inertia, I_y = major axis second moments of inertia; I_z = minor axis second moment of inertia; J = torsional rigidity. The origin is denoted by (O) and is located at the left hand corner of the flange. The spacings of the ribs are also denoted by sp^{Li}, and sp^{Ti}, as shown in the figure. It must be noted that the geometric properties of the ribs are computed for the T-profile without participation from the flange or the web.
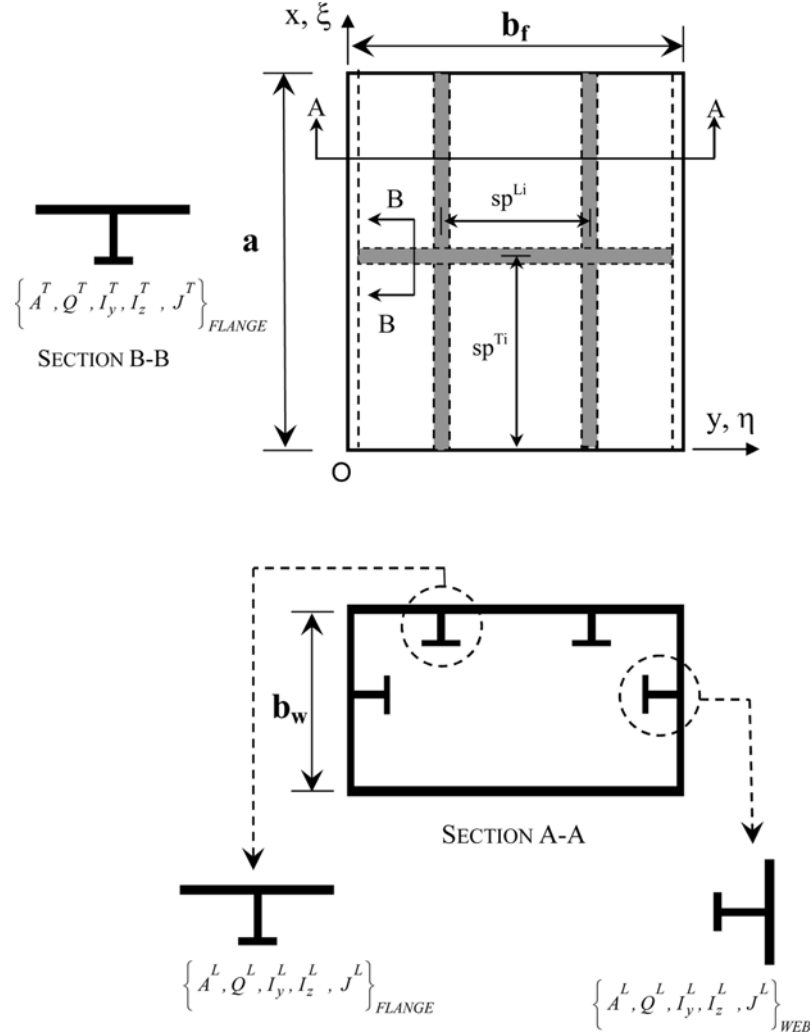
Fig. 3 Details of typical stiffened support details

In the present formulation the flanges are treated as partially restrained against rotation and in-plane translation. This represents intermediate boundary condition between the extreme simply supported and clamped boundaries. The intensity of the flange restraints are dictated by the geometric properties of the web. Similar treatments are accorded to the longitudinal edges of the webs. By treating the flange as single plate element, the out-of plane deflection function can be assumed in the following form

$$W^f(\eta, \xi) = \sum_{i=1}^{M_1}\sum_{j=1}^{N_1} b_{ij}^f P_i^f(\xi)\Omega_j(\eta) \tag{1}$$

Where $P_i(\xi)$ and $\Omega_j(\eta)$, describe flange longitudinal and transverse displacement profiles, respectively. ξ and η are non-dimensional parameters, given by $\xi = x/a$ and $\eta = y/b_f$. In the present

formulation, the out of plane deflection of the flange at the web/flange junction is assumed to be zero. It is further assumed that local buckling of the ribs will not occur prior to the flange or the web. Also, the torsional rigidity of the stiffeners is estimated by St. Venant's theory.

When using the compatibility conditions (at $\eta = 0, 1$) along the web/flange junctions, $\Omega_j(\eta)$ can be expressed as

$$\Omega_j(\eta) = 2(1 - v)\left(\frac{b_f}{a}\right)\left(\frac{b_w}{t_f}\right)^3\left(\frac{t_w}{a}\right)\left[\frac{\partial \omega_j^{f2}(\eta)}{\partial \eta}\left(\frac{\partial^2 \omega_j^{f1}(\eta)}{\partial \eta^2}\right)^{-1}\right]_{(\eta = 0, 1)} \omega_j^{f1}(\eta) + \omega_j^{f2}(\eta) \tag{2}$$

Note that the function $\Omega_j(\eta)$ relates the flange and the web geometric parameters. The displacement functions $\omega_j^{f1}(\eta)$ needs to satisfy the rotationally clamped condition, while $\omega_j^{f2}(\eta)$ needs to satisfy the rotationally free boundary condition at web/flange junctions ($\eta = 0, 1$).

In the presented formulation, the transverse edges ($\xi = 0$ and 1) are treated as either simply supported or clamped. Accordingly, the function $P_{ij}^f(\xi)$ needs to satisfy in addition to zero out-of plane deflection, either zero moment or slope, i.e.

$$[P_{ij}^f(\xi)]_{(\xi = 0, 1)} = 0, \quad \left[\frac{\partial P_{ij}^f(\xi)}{\partial \xi}\right]_{(\xi = 0, 1)} = 0 \tag{3}$$

or

$$[P_{ij}^f(\xi)]_{(\xi = 0, 1)} = 0, \quad \left[\frac{\partial^2 P_{ij}^f(\xi)}{\partial \xi^2}\right]_{(\xi = 0, 1)} = 0 \tag{4}$$

The flange in-plane displacement functions (U^f and V^f) are expressed as

$$U^f(\xi, \eta) = \sum_{m=1}^{M_2} \sum_{n=1}^{N_2} u_{mn}^f \Phi_m(\xi) Y_n(\eta) \tag{5}$$

$$V^f(\xi, \eta) = \sum_{r=1}^{M_3} \sum_{s=1}^{N_3} v_{rs}^f Z_r(\xi) H_s(\eta) \tag{6}$$

When using Eqs. (1)-(6), the strain energy Π^f, of the flange can be expressed in the following form

$$\Pi^f = \begin{bmatrix} \mathbf{F}_{mnpq} & \mathbf{F}_{mnrs} & \mathbf{F}_{mnijkl} & \mathbf{F}_{ijkltfze} & \mathbf{F}_{rsgh} & \mathbf{F}_{rsijkl} & \mathbf{F}_{ijkl} \end{bmatrix} \begin{bmatrix} u_{mn}^f u_{pq}^f \\ u_{mn}^f v_{rs}^f \\ u_{mn}^f \\ v_{rs}^f v_{gh}^f \\ v_{rs}^f \end{bmatrix} \tag{7}$$

The expressions for the integral functions [**F**] are provided in Appendix I. Similarly, the strain energy of typical longitudinal rib can be expressed as

$$\Pi_{st}^{Li} = [S_{ijkl}^{Li} \ \ S_{ijmn}^{Li} \ \ S_{ijmnkl}^{Li} \ \ S_{ijkltfze}^{Li} \ \ S_{ijkltf}^{Li} \ \ S_{mnpq}^{Li} \ \ S_{rsgh}^{Li}] \begin{bmatrix} b_{ij}^f b_{kl}^f \\ u_{mn}^f b_{ij}^f \\ b_{ij}^f u_{mn}^f b_{kl}^f \\ b_{ij}^f b_{kl}^f b_{tf}^f b_{ze}^f \\ b_{ij}^f b_{kl}^f b_{tf}^f \\ u_{mn}^f u_{pq}^f \\ v_{rs}^f u_{gh}^f \end{bmatrix} \tag{8}$$

Note that the superscripts denote the rib direction and subscripts denote the summation. The matrices [**S^{Li}**] contain the geometric parameters of the ribs and are provided in the Appendix I. Similarly the strain energy of typical transverse rib is given by

$$\Pi_{st}^{Ti} = [S_{ijkl}^{Ti} \ \ S_{ijrs}^{Ti} \ \ S_{ijrskl}^{Ti} \ \ S_{ijkltfze}^{Ti} \ \ S_{ijkltf}^{Ti} \ \ S_{mnpq}^{Ti} \ \ S_{rsgh}^{Ti}] \begin{bmatrix} b_{ij}^f b_{kl}^f \\ v_{rs}^f b_{ij}^f \\ b_{ij}^f v_{rs}^f b_{kl}^f \\ b_{ij}^f b_{kl}^f b_{tf}^f b_{ze}^f \\ b_{ij}^f b_{kl}^f b_{tf}^f \\ u_{mn}^f u_{pq}^f \\ v_{rs}^f u_{gh}^f \end{bmatrix} \tag{9}$$

The expressions for the integral functions [**S^{Ti}**] are given in Appendix I.

Beside the rotational restraint, the attached webs (or diaphragms) also restrain the flange laterally against in-plane motion. As the flange is compressed axially, the longitudinal edges (at $\xi = 0,1$) will expand in the perpendicular direction due to the Poisson effect. However, the webs (or diaphragms) will resist this in-plane motion. The two extreme conditions are free in-plane motion or fully restrained against in-plane translation. If, in the analysis, the flange is considered to be restrained against in-plane translation, the strain ($\varepsilon_y = 0$) at $\xi = 0$ and 1. As a result, additional destabilizing forces will appear in the transverse direction that will lower the buckling load. If the webs are stiffened, the intensity of this restrain will be more pronounced on the flange. The work done by the applied and the applied and induced forces due to lateral restraint, is given by

$$V = \left[V_{ijkl}^1 \ \ \sum_{i=1}^{NS^{Li}} V_{ijkl}^2 \ \ \sum_{i=1}^{NS^{Li}} V_{ijkl}^3 \right] \begin{bmatrix} N^f \\ N^{Li} \\ N^{Ti} \end{bmatrix} b_{ij}^f b_{kl}^f \tag{10}$$

Where

$$V^1_{ijkl} = \sum_{i=1}^{M_2}\sum_{j=1}^{N_2}\sum_{k=1}^{M_2}\sum_{l=1}^{N_2}\int_0^1\int_0^1\left[\frac{b_f}{a}\frac{\partial P_i(\xi)}{\partial \xi}\frac{\partial P_k(\xi)}{\partial \xi}\Omega_j(\eta)\Omega_l(\eta)+\nu\frac{t_w b_w/t_f b_f}{1+(t_w b_w/t_f b_f)}\frac{a_f}{b_f}P_k(\xi)P_i(\xi)\frac{\partial \Omega_j(\eta)}{\partial \eta}\frac{\partial \Omega_l(\eta)}{\partial \eta}\right]d\xi d\eta \tag{11}$$

$$V^2_{ijkl} = \frac{A^{Xi}}{2t_f a}\sum_{i=1}^{M_2}\sum_{j=1}^{N_2}\sum_{k=1}^{M_2}\sum_{l=1}^{N_2}\int_0^1\frac{\partial P_i(\xi)}{\partial \xi}\frac{\partial P_k(\xi)}{\partial \xi}\Omega_j(\eta)\Omega_l(\eta)d\xi \tag{12}$$

$$V^3_{ijkl} = \nu A^{Yi}\frac{t_w b_w/t_f b_f}{t_f b_f + t_w b_w}\sum_{i=1}^{M_2}\sum_{j=1}^{N_2}\sum_{k=1}^{M_2}\sum_{l=1}^{N_2}\int_0^1 P_i(\xi)P_k(\eta)\frac{\partial \Omega_j(\eta)}{\partial \eta}\frac{\partial \Omega_l(\eta)}{\partial \eta}d\eta \tag{13}$$

By assembling the potential energy components, and minimizing with respect to the displacement coefficients $\{b_{ij},\ u_{mn},\ v_{rs}\}$, the buckling stress of the flange can be expressed as

$$\sigma^f_{cr} = K^f(b^f_{ij}, u^f_{mn}, v^f_{rs})\frac{\pi^2 E}{12(1-\nu^2)}\left(\frac{t_f}{b_f}\right)^2 \tag{14}$$

Note that K_f is the parameter that contains the $[\mathbf{F}]$, $[\mathbf{S}^{Xi}_{st}]$, $[\mathbf{S}^{Yi}_{st}]$ and $[\mathbf{V}]$ integrals which are function of the flange, web, stiffeners properties and shape functions $\{P_i(\xi),\ \omega_j(\eta),\ \Phi_m(\xi),\ Y_n(\eta),\ Z_r(\xi),\ H_s(\eta)\}$. By similar analogy, the buckling stress of the web can be expressed in similar format

$$\sigma^w_{cr} = K^w(b^w_{ij}, u^w_{mn}, v^w_{rs})\frac{\pi^2 E}{12(1-\nu^2)}\left(\frac{t_w}{b_w}\right)^2 \tag{15}$$

Since these parameters are non-linear function of these coefficients, analytical treatment of the problem becomes difficult. In this study, non-linear programming techniques were employed to determine the critical stress for the box girder components. The solution procedure for the mathematical algorithm is described by Schittkowski (1985). In this problem, the objective is to find the coefficients $\{b_{ij},\ u_{mn},\ v_{rs}\}$ that minimize the flange/web buckling coefficients $(K^{w,f})$. The mathematical statement of the unconstrained optimization problem is stated as follow

$$\text{Minimize} \quad K^{f,w}(b_{ij}, u_{mn}, v_{rs}) \tag{16}$$

The solution strategy for the non-linear function is performed iteratively by generating and solving a sequence of Quadratic sub-problems. Each iteration is described a step size and search direction that are computed to produce a sufficient decrease in the objective function. The process continues until there is no further decrease in the objective function or the decrease is of negligible order.

3. Numerical results

3.1 Unstiffened box girder supports (Uniform Compression)

To illustrate the geometric interaction, unstiffened box girder is first considered. The variations of the buckling curves for the flange and the web are presented in the graphical format shown in Fig. 4. The buckling coefficient $(K^{f,w})$ is plotted versus the flange/web thickness (t_f/t_w) for several

(b_f/b_w) ratios. Note that the buckling curves for each (b_f/b_w) ratio are plotted using the same legend. To maintain clarity of the figure, the continuations of these curves beyond their points of intersection are not shown. Therefore, the stability domain for each (b_f/b_w) is the area under these intersecting curves. The solid curves represent (b_f/b_w) = 1, the dotted represent (b_f/b_w) = 2 and the dashed represent (b_f/b_w) = 4. Points of intersection represent the values at which the webs and the flange buckle simultaneously. These points correspond to the optimum flange/web geometric proportions that maximize the buckling load. The lower and upper limiting conditions are also identified in the figure. Since the relative geometric proportions of the web and the flange dictate the intensities of these restraints, their "true buckling coefficients lie within the limiting conditions. As shown, when (b_f/b_w) = 1, the flange dominates buckling load for in the range (t_f/t_w) ≥ 1. For smaller (t_f/t_w) values, the web buckles before the flange. Similarly, for (b_f/b_w) = 2, the flange buckles before the web for (t_f/t_w) ≥ 0.86. It can be observed that the optimum ($K^{f,w}$) value for the box section occur at different (t_w/t_f) ratios. For example, when (b_f/b_w) = 1 the optimum K occurs at (t_f/t_w) = 1. This is because, the flange and the web have identical restraints (rotational and lateral). Therefore, increasing (b_f/b_w) ratio requires lower (t_f/t_w) value to reach the optimum ($K^{f,w}$). For example, when (b_f/b_w) = 2, the optimum ($K^{f,w}$) is achieved at (t_f/t_w) = 0.83. By further increasing (b_f/b_w) to 4 the optimum ($K^{f,w}$) value is attained at (t_f/t_w) = 0.73.

The form of this graph very useful to use in practice to provide an economical design for the box girder supports. For example, if the designer decides to use a flange width of b_f = 1200 mm, web width b_w = 600 mm, and web thickness of (t_w) = 12 mm. The optimum flange thickness required in this case is (t_f) = 10 mm. If alternatively, the thickness of the flanges and the web is dictated by the steel fabricators by (t_f) = 8 mm and (t_w) = 10 mm. Then, by using a flange width of 1600 mm, the optimum web width is 400 mm.

Fig. 5 shows the variation of the flange buckling coefficient (K^f) with (b_f/b_w) for un-stiffened box. The figure shows the change in the flange buckling coefficient (K^f) by modifying (b_f/b_w) and (t_f/t_w) ratios. The solid curve represents (t_f/t_w) = 2; the dotted curve represents (t_f/t_w) = 1.5 and the dashed curve represents (t_f/t_w) = 1.25. It can be observed that the decrease in the flange buckling coefficient occurs when (b_f/b_w) ≤ 0.65. For larger values, the decrease in (K^f) is much slower. Further increase
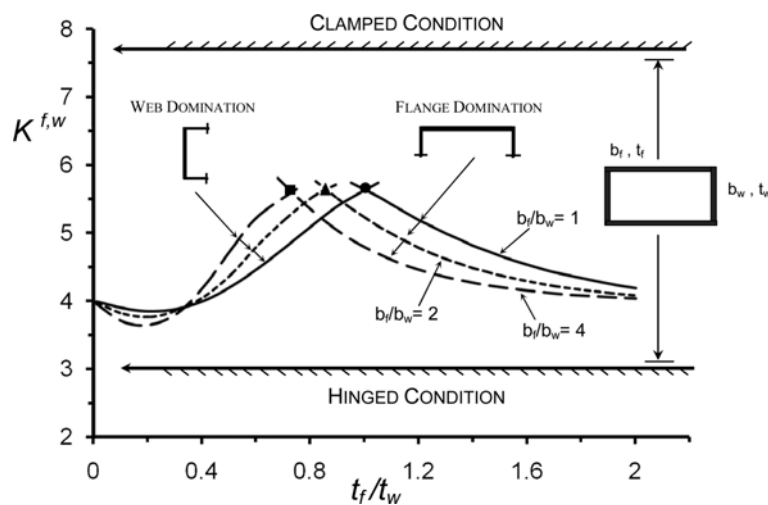

Fig. 4 Variation of $K^{f,w}$, with (t_f/t_w) for unstiffened box section
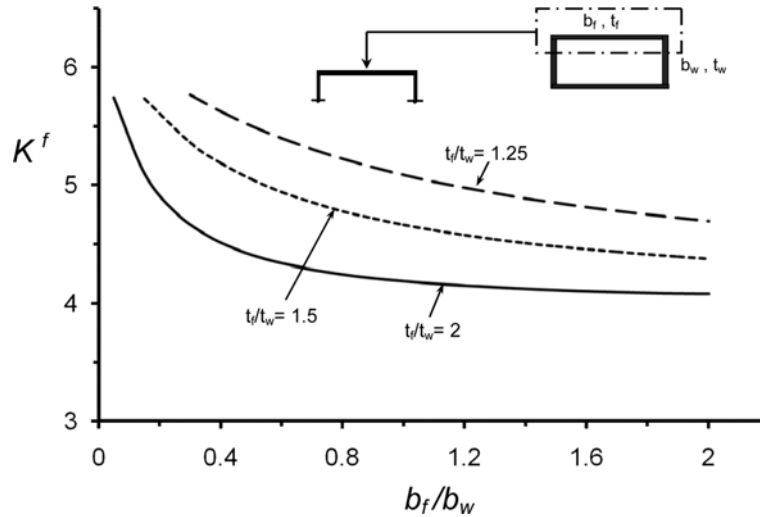
Fig. 5 Variation of K^f with (b_f/b_w) for unstiffened box section

in (b_f/b_w) has slight effect on the flange buckling load. Although in this example the webs did not dominate the buckling load, the change in their geometric sizes influenced the flange stability.

3.2 Stiffened box girder supports

A computer program was developed to compute the buckling stress of stiffened box girders. For given rib cross sectional properties and spacing, the program computes the buckling stress. Geometric detail of the next case study is shown in Fig. 6. In this example, the flanges and the webs are stiffened in the longitudinal and transverse directions by T-stiffeners along the centrelines, i.e., for the flange $\{sp^{L1} = b_f/2, sp^{T1} = a/2\}$ and for the web $\{sp^{L1} = b_w/2, sp^{T1} = a/2\}$. The dimensions of the longitudinal rib are; depth = 53 mm, flange width = 103 mm, flange thickness = 8.8 mm and stem thickness = 7.1 mm. The dimensions of the transverse rib are; depth = 103 mm, flange width = 102 mm; flange thickness = 8 mm and stem thickness = 6.2 mm. The stability design space for the box girder support is shown in Fig. 7. The flange/web thickness ratio (t_f/t_w) ranges between 0.5-2.0. The web is subject to variable flexural load ranging between $\sigma_1/\sigma_2 = -1, -0.5, 0, 0.5, 1$.

The solid triangles are used to identify the web curves, while solid circles are used to identify the flange curves. Note that the solid segments in curves corresponding $(\sigma_1/\sigma_2) = 1, 0.5$ represent the web domination and the dashed segments represent the inactive part. It can be seen that as the stress ratios increases the buckling stress decreases. Also the web buckling stress varies significantly by modifying the flange geometric properties. For $(\sigma_1/\sigma_2) = -1$, for examples, the web buckling coefficient (K^w) varies between 19.2-29 by changing the flange/web thickness ratio (t_f/t_w) from 0.5 to 2. Similarly, when the stress ratio $(\sigma_1/\sigma_2) = 0$, the web buckling coefficient (K^w) varies between 15-21. This shows the influence of the flange/web geometric proportions on the behaviour of the box girder supports.

Geometric detail of the second stiffened box girder support is shown in Fig. 8. In this case, the flange and web stiffening profiles are different. The webs are stiffened in the longitudinal direction by two equally spaced T-stiffeners at $sp^{L1} = sp^{L2} = b_w/3$. The web stiffener depth = 53 mm, flange
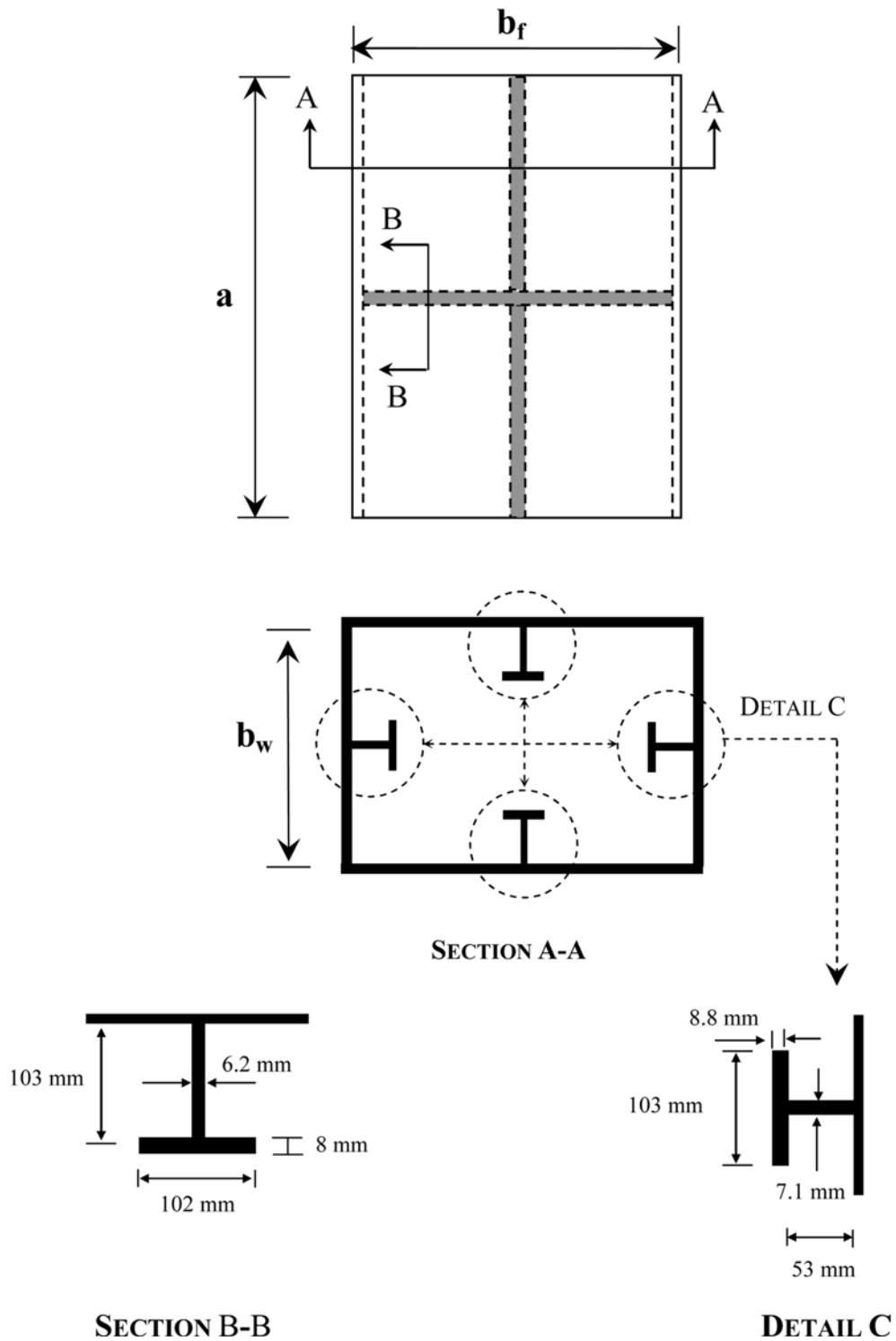
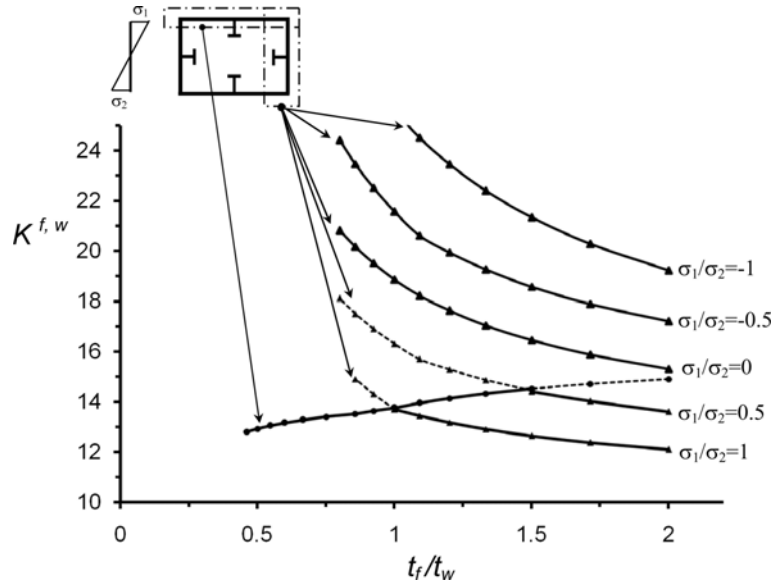Fig. 6 Geometric details of stiffened box- section support example 1

Fig. 7 Variation of $K^{f,w}$ with (t_f/t_w) for stiffened box section example 1

width = 103 mm, flange thickness = 8.8 mm and stem thickness = 7.1 mm. In the transverse direction the web is stiffened at the centreline ($sp^{T1} = a/2$). The web transverse stiffener depth = 103 mm, flange width = 102 mm; flange thickness 8 mm and stem thickness = 6.2 mm. The flange is stiffened in the transverse direction (as shown by section B-B) by central T-stiffener at $sp^{T1} = a/2$ with geometric dimensions identical to the web stiffener. In the longitudinal direction, the flange is stiffened by identical rectangular ribs with depth = 50 mm and thickness = 4 mm. Modulus of Elasticity and Poisson's ratio of the section are $E = 200$ GPa and $v = 0.33$.

Fig. 9 shows the variation of the flange buckling stress (σ^f_{cr}) with (t_f/t_w) for the stiffened box girder. The dotted curve represents flange with four ribs ($sp^{L1} = sp^{L2} = sp^{L3} = sp^{L4} = b_f/5$). The dashed curve represents a flange with five ribs ($sp^{L1} = sp^{L2} = sp^{L3} = sp^{L4} = sp^{L5} = b_f/6$). The solid curve represents the flange with six ribs ($sp^{L1} = sp^{L2} = sp^{L3} = sp^{L4} = p^{L5} = sp^{L6} = b_f/7$). It can be observed that the increase in the curves becomes sharper in the early stage as the number of ribs increases. For example, by fixing (t_f/t_w) = 0.7, the flange buckling stress (σ^f_{cr}) = 203 MPa. when using four ribs. The flange buckling stress value increases to (σ^f_{cr}) = 219 MPa by adding a fifth rib. The value of (σ^f_{cr}) = 233 MPa by using six ribs. It should be indicated that the upper and lower limiting conditions for the flange with six ribs are (σ^f_{cr}) = 250 MPa and 209 MPa, respectively. The bounds for flange with five ribs are {230 MPa, 203 MPa}; and equals to {210 MPa, 190 MPa} for flange with four ribs. Therefore, the variations in the buckling stress are very pronounced in this example due to the interaction between the flange and the web. Although the webs did not dominate the buckling load, the restraints they imposed to the flange are quite significant. As illustration, for flange with six ribs the difference in the buckling stress is almost (20%).

It can also be observed from this example the significant enhancements the ribs induce to the buckling strength of the flange with almost negligible weight to the overall structure. The weight of each rib in this example is almost 1% of the overall weight. By adding two ribs (i.e., increase the weight by 2%), the buckling stress of the flange is increased by almost 18%. To further illustrate
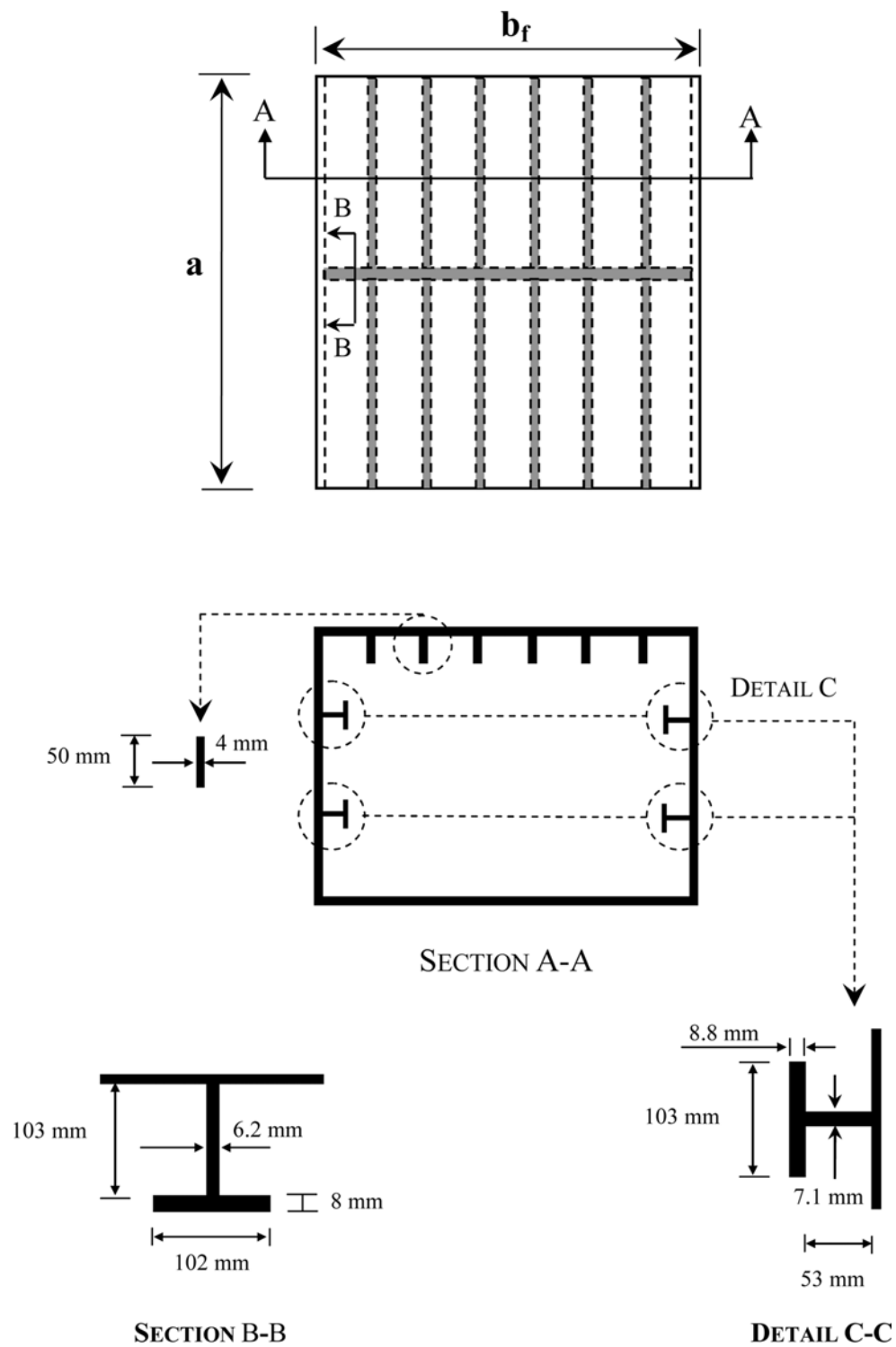
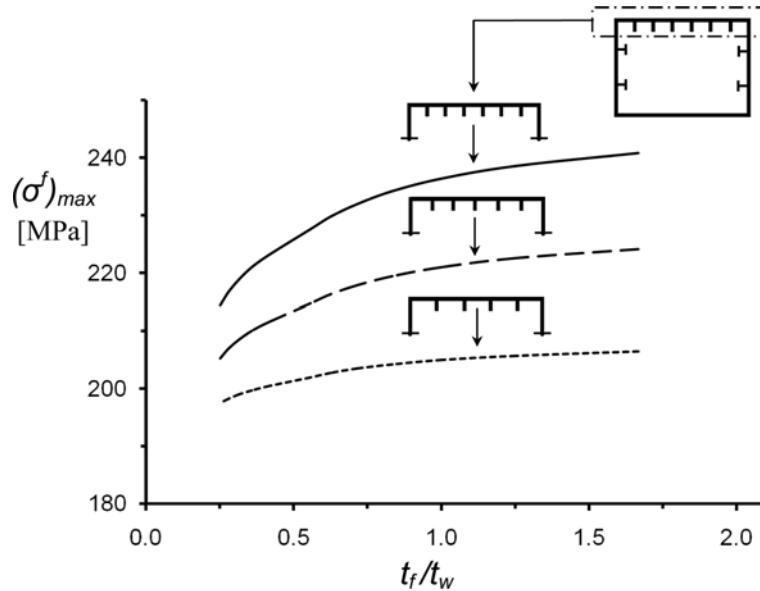Fig. 8 Geometric details of stiffened box-section support example 2

Fig. 9 Variation of $(\sigma^f)_{max}$ with (t_f/t_w) for stiffened box section example 2

the efficiency of the stiffened box system, assume that it is required to design flange for a buckling stress of 245 MPa. By using six stiffeners, the overall weight of the box girder to achieve this stress level is approximately 6.2 tons. If this buckling stress to be achieved without using longitudinal ribs, then the weight of the box girder should increase to 9.2 tons by adjusting the flange thickness. This corresponds to almost 55% increase in weight.

4. Conclusions

The paper highlighted the influence of the flange/web geometric proportions on the buckling stress of stiffened box girders. A numerical procedure was presented for the analysis of box girder supports that accounts for the geometric interactions between the webs and the flange. It was shown the buckling stress may vary by 20% if the web/flange interaction is not properly accounted for. Graphs were presented for several box girder supports to identify the stability design space. The variation of the buckling stresses with the web/flange thickness ratios (t_f/t_w) was shown for various stiffening configurations. It was shown that the buckling strength of the flange is largely affected by the restraints imposed by the webs. These graphs are useful to use in practice in order to achieve economical and efficient design of box girders.

References

Barik, M. and Mukhopadhyay, M. (2002), "A new stiffened plate element for the analysis of arbitrary plates", *Thin Wall. Struct.*, **40**, 625-632.
Bhar, A., Phoenix, S.S. and Satsangi, S.K. (2010), "Finite element analysis of laminated composite stiffened

plates using FSDT and HSDT: A comparative perspective", *Compos. Struct.*, **92**(2), 312-321.

Bonorchis, D. and Nurick, G.N. (2010), "The analysis and simulation of welded stiffener plates subjected to localised blast loading", *J. Impact Eng.*, **37**(3), 260-273.

He, J. and He, G. (2010), "Strength analysis of composite grid stiffened structure", *J. Solid Rocket Tech.,* **33**(4), 449-453.

Hegaze, M.M. (2010), "Nonlinear dynamic analysis of stiffened and unstiffened laminated composite plates using a high-order element", *J. Compos. Mater.*, **44**(3), 327-346.

Huang, D.T. (2009), "A point receptance array approach for stiffened panel structures", *Int. J. Mech. Sci.*, **52**(10), 1299-1312.

Jiang, Z., Bai, Z., Yan, B. and Song, D. (2010), "Advances in study on impact response of thin and stiffened metal plates under blast loading", *J. Vib. Shock*, **29**(11), 41-46.

Li, L. and Xiaohui, R. (2010), "Stiffened plate bending analysis in terms of refined triangular laminated plate element", *Compos. Struct.*, **92**(12), 2936-2945.

Mallela, U. and Upadhyay, A. (2006), "Buckling of laminated composite stiffened panels subjected to in-plane shear: A parametric study", *Thin Wall. Struct.*, **44**, 354-361.

Nath, S.K.D., Ahmed, S.R. and Kim, S. (2010), "Analytical solution of a stiffened orthotropic plate using alternative displacement potential approach", *Proceedings of the Institution of Mechanical Engineers, Part G: Journal of Aerospace Engineering*, **224**(1), 89-99.

Patel, S., Datta, P. and Sheikh, A. (2006), "Buckling and dynamic instability analysis of stiffened shell panels", *Thin Wall. Struct.*, **44**, 321-333.

Rikards, R., Chate, A. and Ozolinsh, O. (2001), "Analysis for buckling and vibrations of composite stiffened shells and plates", *Compos. Struct.*, **51**, 361-370.

Schittkowski, K. (1985), "A unified outline of non-linear programming algorithms", *J. Mech. Trans. Auto. D.,* **107**, 449-453.

Stamatelos, D.G., Labeas, G.N. and Tserpes, K.I. (2011), "Analytical calculation of local buckling and post-buckling behavior of isotropic and orthotropic stiffened panels", *Thin Wall. Struct.*, **49**(3), 422-430.

Tamijani, A.Y. and Kapania, R.K. (2010), "Buckling and vibration of curvilinearly-stiffened plate subjected to in-plane loads using Chebyshev ritz method", *Proceedings of the 51st AIAA/ASME/ASCE/AHS/ASC Structures, Structural Dynamics and Materials Conference*, 2010-3036.

Zhang, Z., Chen, H. and Ye, L. (2011), "A stiffened plate element model for advanced grid stiffened composite plates/shells", *J. Compos. Mater.*, **45**, 187-202.

Zhang, Z.H., Xiao, C., Chen, L., Wang, C. and Huang, Y. (2010), "Approximate scaling method of stiffened plate subjected to underwater explosion blast", *J. Ship Mech.*, **14**(11), 1276-1283.

Zhang, W., Wang, A., Vlahopoulos, N. and Wu, K. (2005), "Vibration analysis of stiffened plates under heavy fluid loading by an energy finite element analysis formulation", *Finite Elem. Analy. Des.*, **41**, 1056-1078.

Appendix. I

The expressions for the integral functions $[F]$, $[S^{Li}]$ and $[S^{Ti}]$ are given by

$$F_{mnpq} = \frac{Et_f}{2(1-v^2)}\sum_{m=1}^{M_1}\sum_{n=1}^{N_1}\sum_{p=1}^{M_3}\sum_{q=1}^{N_3}\int_0^1\int_0^1\left[\frac{b_f}{a}\frac{\partial\Phi_m(\xi)}{\partial\xi}\frac{\partial\Phi_p(\xi)}{\partial\xi}Y_n(\eta)Y_q(\eta)+(1-v)\frac{a}{2b_f}\Phi_m(\xi)\Phi_p(\xi)\frac{\partial Y_n(\eta)}{\partial\eta}\frac{\partial Y_q(\eta)}{\partial\eta}\right]d\xi d\eta$$

(A-1)

$$F_{mnrs} = \frac{Et_f}{2(1-v^2)}\sum_{m=1}^{M_2}\sum_{n=1}^{N_2}\sum_{r=1}^{M_3}\sum_{s=1}^{N_3}\int_0^1\int_0^1\left[2v\frac{\partial\Phi_m(\xi)}{\partial\xi}Z_r(\xi)Y_n(\eta)\frac{\partial H_s(\eta)}{\partial\eta}+(1-v)\Phi_m(\xi)\frac{\partial Z_r(\xi)}{\partial\xi}\frac{\partial Y_n(\eta)}{\partial\eta}H_s(\eta)\right]d\xi d\eta$$ (A-2)

$$F_{mnijkl} = \frac{Et_f}{2(1-v^2)}\sum_{m=1}^{M_2}\sum_{n=1}^{N_2}\sum_{i=1}^{M_1}\sum_{j=1}^{N_1}\sum_{k=1}^{M_2}\sum_{l=1}^{N_2}\int_0^1\int_0^1\left[\frac{b_f}{a^2}\frac{\partial\Phi_m(\xi)}{\partial\xi}\frac{\partial P_i(\xi)}{\partial\xi}\frac{\partial P_k(\xi)}{\partial\xi}Y_n(\eta)\Omega_j(\eta)\Omega_l(\eta)+\frac{v\partial\Phi_m(\xi)}{b_f\partial\xi}P_i(\xi)P_k(\xi)P_n(\eta)\right.$$

$$\left.\frac{\partial\Omega_j(\eta)}{\partial\eta}\frac{\partial\Omega_l(\eta)}{\partial\eta}+\frac{1-v}{b_f}\Phi_m(\xi)\frac{\partial P_i(\xi)}{\partial\xi}P_k(\xi)\frac{\partial Y_n(\eta)}{\partial\eta}\Omega_j(\eta)\frac{\partial\Omega_l(\eta)}{\partial\eta}\right]d\xi d\eta$$

(A-3)

$$F_{ijklftze} = \frac{Et_f}{2(1-v^2)}\sum_{i=1}^{M_1}\sum_{j=1}^{N_1}\sum_{k=1}^{M_2}\sum_{l=1}^{N_2}\sum_{f=1}^{M_2}\sum_{t=1}^{N_2}\sum_{z=1}^{M_2}\sum_{e=1}^{N_2}\int_0^1\int_0^1\left[\frac{b_f}{4a^3}\frac{\partial P_i(\xi)}{\partial\xi}\frac{\partial P_k(\xi)}{\partial\xi}\frac{\partial P_l(\xi)}{\partial\xi}\frac{\partial P_z(\xi)}{\partial\xi}\Omega_j(\eta)\Omega_l(\eta)\Omega_f(\eta)\Omega_e(\eta)+\right.$$

$$\frac{a_f}{4b_f^3}P_i(\xi)P_k(\xi)P_l(\xi)P_z(\xi)\frac{\partial\Omega_j(\eta)}{\partial\eta}\frac{\partial\Omega_l(\eta)}{\partial\eta}\frac{\partial\Omega_f(\eta)}{\partial\eta}\frac{\partial\Omega_e(\eta)}{\partial\eta}+$$

$$\left.\frac{1}{2ab_f}\frac{\partial P_i(\xi)}{\partial\xi}\frac{\partial P_k(\xi)}{\partial\xi}\frac{\partial P_l(\xi)}{\partial\xi}\frac{\partial P_z(\xi)}{\partial\xi}\frac{\partial\Omega_j(\eta)}{\partial\eta}\frac{\partial\Omega_l(\eta)}{\partial\eta}\frac{\partial\Omega_f(\eta)}{\partial\eta}\frac{\partial\Omega_e(\eta)}{\partial\eta}\right]d\xi d\eta$$

(A-4)

$$F_{rsgh} = \frac{Et_f}{2(1-v^2)}\sum_{r=1}^{M_3}\sum_{s=1}^{N_3}\sum_{g=1}^{M_3}\sum_{h=1}^{N_3}\int_0^1\int_0^1\left[\frac{a}{b_f}Z_r(x)Z_g(\xi)\frac{\partial H_s(\eta)}{\partial\eta}\frac{\partial H_h(\eta)}{\partial\eta}+\frac{b_f}{a}\frac{1-v}{2}\frac{\partial Z_r(\xi)}{\partial\xi}\frac{\partial Z_g(\xi)}{\partial\xi}H_s(\eta)H_h(\eta)\right]d\xi d\eta$$ (A-5)

$$F_{rsijkl} = \frac{Et_f}{2(1-v^2)}\sum_{r=1}^{M_3}\sum_{s=1}^{N_3}\sum_{i=1}^{M_2}\sum_{j=1}^{N_2}\sum_{k=1}^{M_2}\sum_{l=1}^{N_2}\int_0^1\int_0^1\left[\frac{a}{b_f}Z_r(\xi)P_i(\xi)P_k(\xi)\frac{\partial H_s(\eta)}{\partial\eta}\frac{\partial\Omega_j(\eta)}{\partial\eta}\frac{\partial\Omega_l(\eta)}{\partial\eta}+\frac{v}{a}Z_r(\xi)\frac{\partial P_i(\xi)}{\partial\xi}\frac{\partial P_k(\xi)}{\partial\xi}\frac{\partial H_s(\eta)}{\partial\eta}\right.$$

$$\left.\Omega_j(\eta)\Omega_l(\eta)+\frac{1-v}{a}\frac{\partial Z_r(\xi)}{\partial\xi}\frac{\partial Z_i(\xi)}{\partial\xi}P_k(\xi)H_s(\eta)\Omega_j(\eta)\frac{\partial\Omega_l(\eta)}{\partial\eta}\right]d\xi d\eta$$

(A-6)

$$F_{ijkl} = \frac{Et_f^3}{24(1-v^2)}\sum_{i=1}^{M_1}\sum_{j=1}^{N_1}\sum_{k=1}^{M_2}\sum_{l=1}^{N_2}\int_0^1\int_0^1\left[\frac{b_f^2}{a^2}\frac{\partial^2 P_i(\xi)}{\partial\xi^2}\frac{\partial^2 P_k(\xi)}{\partial\xi^2}\Omega_j(\eta)\Omega_l(\eta)+\frac{a^3}{4b_f^3}P_i(\xi)P_k(\xi)\frac{\partial^2\Omega_j(\eta)}{\partial\eta^2}\frac{\partial^2\Omega_l(\eta)}{\partial\eta^2}+2v\frac{\partial^2 P_i(\xi)}{\partial^2\xi}\frac{\partial^2 P_k(\xi)}{\partial\xi^2}\right.$$

$$\left.\frac{\partial^2\Omega_j(\eta)}{\partial\eta^2}\frac{\partial^2\Omega_l(\eta)}{\partial\eta^2}+2(1-v)\frac{\partial P_i(\xi)}{\partial\xi}\frac{\partial P_k(\xi)}{\partial\xi}\frac{\partial\Omega_j(\eta)}{\partial\eta}\frac{\partial\Omega_l(\eta)}{\partial\eta}\right]d\xi d\eta$$

(A-7)

$$S^{Li}_{ijkl} = \frac{E}{2}\sum_{i=1}^{M_1}\sum_{j=1}^{N_1}\sum_{k=1}^{M_2}\sum_{l=1}^{N_2}\int_0^1\left[\frac{I_y^{Li}}{a^3}\frac{\partial^2 P_i(\xi)}{\partial\xi^2}\frac{\partial^2 P_k(\xi)}{\partial\xi^2}\Omega_j(\eta)\Omega_l(\eta)+\frac{1}{2(1+v)}\frac{J^{Li}}{b_f^3}\frac{\partial P_i(\xi)}{\partial\xi}\frac{\partial P_k(\xi)}{\partial\xi}\frac{\partial\Omega_j(\eta)}{\partial\eta}\frac{\partial\Omega_l(\eta)}{\partial\eta}\right]d\xi$$

$$S^{Li}_{ijmn} = -\frac{EQ^{Li}}{a^2}\sum_{i=1}^{M_1}\sum_{j=1}^{N_1}\sum_{m=1}^{M_2}\sum_{n=1}^{N_2}\int_0^1\frac{\partial\Phi_m(\xi)}{\partial\xi}\frac{\partial^2 P_i(\xi)}{\partial\xi^2}Y_n(\eta)\Omega_j(\eta)d\xi$$ (A-8)

$$S^{Li}_{ijmnkl} = \frac{EA^{Li}}{2a^2}\sum_{i=1}^{M_1}\sum_{j=1}^{N_1}\sum_{m=1}^{M_2}\sum_{n=1}^{N_2}\sum_{k=1}^{M_2}\sum_{l=1}^{N_2}\int_0^1\frac{\partial\Phi_m(\xi)}{\partial\xi}\frac{\partial P_i(\xi)}{\partial\xi}\frac{\partial P_k(\xi)}{\partial\xi}Y_n(\eta)\Omega_j(\eta)\Omega_l(\eta)d\xi$$ (A-9)

$$S^{Li}_{ijkltze} = \frac{EA^{Li}}{8a^3}\sum_{i=1}^{M_1}\sum_{j=1}^{N_1}\sum_{k=1}^{M_2}\sum_{l=1}^{N_2}\sum_{f=1}^{M_2}\sum_{z=1}^{N_2}\sum_{t=1}^{M_2}\sum_{e=1}^{N_2}\int_0^1\frac{\partial P_i(\xi)}{\partial\xi}\frac{\partial P_k(\xi)}{\partial\xi}\frac{\partial P_l(\xi)}{\partial\xi}\frac{\partial P_z(\xi)}{\partial\xi}\Omega_j(\eta)\Omega_l(\eta)\Omega_f(\eta)\Omega_e(\eta)d\xi$$ (A-10)

$$S_{ijkltf}^{Li} = \frac{EQ}{2a^3} \sum_{i=1}^{M_1} \sum_{j=1}^{N_1} \sum_{k=1}^{M_2} \sum_{l=1}^{N_2} \sum_{t=1}^{M_2} \sum_{f=1}^{N_2} \int_0^1 \frac{\partial^2 P_i(\xi)}{\partial \xi^2} \frac{\partial P_k(\xi)}{\partial \xi} \frac{\partial P_t(\xi)}{\partial \xi} \Omega_j(\eta) \Omega_l(\eta) \Omega_f(\eta) d\xi \tag{A-11}$$

$$S_{mnpq}^{Li} = \frac{EA}{2a} \sum_{m=1}^{M_2} \sum_{n=1}^{N_2} \sum_{p=1}^{M_2} \sum_{q=1}^{N_2} \int_0^1 \frac{\partial \Phi_m(\xi)}{\partial \xi} \frac{\partial \Phi_p(\xi)}{\partial \xi} Y_n(\eta) Y_q(\eta) d\xi \tag{A-12}$$

$$S_{rsgh}^{Li} = \frac{EI_z}{2a^3} \sum_{r=1}^{M_2} \sum_{s=1}^{N_2} \sum_{g=1}^{M_2} \sum_{h=1}^{N_2} \int_0^1 \frac{\partial^2 Z_r(\xi)}{\partial \xi^2} \frac{\partial^2 Z_g(\xi)}{\partial \xi^2} H_s(\eta) H_h(\eta) d\xi \tag{A-13}$$

$$S_{ijkl}^{Ti} = \frac{E}{2} \sum_{i=1}^{M_1} \sum_{j=1}^{N_1} \sum_{k=1}^{M_2} \sum_{l=1}^{N_2} \int_0^1 \left[\frac{I_x^{Ti}}{a^3} P_i(\xi) P_k(\xi) \frac{\partial^2 \Omega_j(\eta)}{\partial \eta^2} \frac{\partial^2 \Omega_l(\eta)}{\partial \eta^2} + \frac{1}{2(1+\nu)} \frac{J^{Ti}}{a} \frac{\partial P_i(\xi)}{\partial \xi} \frac{\partial P_k(\xi)}{\partial \xi} \frac{\partial \Omega_j(\eta)}{\partial \eta} \frac{\partial \Omega_l(\eta)}{\partial \eta} \right] d\eta \tag{A-14}$$

$$S_{ijrs}^{Ti} = -\frac{EQ}{b_f^2} \sum_{i=1}^{M_1} \sum_{j=1}^{N_1} \sum_{r=1}^{M_2} \sum_{s=1}^{N_2} \int_0^1 Z_r(\xi) P_i(\xi) \frac{\partial H_s(\eta)}{\partial \eta} \frac{\partial^2 \Omega_l(\eta)}{\partial \eta^2} d\eta \tag{A-15}$$

$$S_{ijrskl}^{Ti} = \frac{EA}{2b_f^2} \sum_{i=1}^{M_1} \sum_{j=1}^{N_1} \sum_{r=1}^{M_2} \sum_{s=1}^{N_2} \sum_{k=1}^{M_2} \sum_{l=1}^{N_2} \int_0^1 Z_r(\xi) P_i(\xi) P_k(\xi) \frac{\partial H_s(\eta)}{\partial \eta} \frac{\partial \Omega_j(\eta)}{\partial \eta} \frac{\partial \Omega_l(\eta)}{\partial \eta} d\eta \tag{A-16}$$

$$S_{jkltfze}^{Ti} = \frac{EA}{8b_f^3} \sum_{i=1}^{M_1} \sum_{j=1}^{N_1} \sum_{k=1}^{M_2} \sum_{l=1}^{N_2} \sum_{t=1}^{M_2} \sum_{f=1}^{N_2} \sum_{z=1}^{M_2} \sum_{e=1}^{N_2} \int_0^1 P_i(\xi) P_k(\xi) P_t(\xi) P_z(\xi) \frac{\partial \Omega_j(\eta)}{\partial \eta} \frac{\partial \Omega_l(\eta)}{\partial \eta} \frac{\partial \Omega_f(\eta)}{\partial \eta} \frac{\partial \Omega_e(\eta)}{\partial \eta} d\eta \tag{A-17}$$

$$S_{jkltf}^{Ti} = \frac{EQ}{2b_f^3} \sum_{i=1}^{M_1} \sum_{j=1}^{N_1} \sum_{k=1}^{M_2} \sum_{l=1}^{N_2} \sum_{t=1}^{M_2} \sum_{f=1}^{N_2} \int_0^1 P_i(\xi) P_k(\xi) P_t(\xi) \frac{\partial^2 \Omega_j(\eta)}{\partial \eta^2} \frac{\partial \Omega_l(\eta)}{\partial \eta} \frac{\partial \Omega_f(\eta)}{\partial \eta} d\eta \tag{A-18}$$

$$S_{mnpq}^{Ti} = \frac{EA}{2b_f} \sum_{m=1}^{M_2} \sum_{n=1}^{N_2} \sum_{p=1}^{M_2} \sum_{q=1}^{N_2} \int_0^1 \Phi_m(\xi) \Phi_p(\xi) \frac{\partial^2 Y_n(\eta)}{\partial \eta^2} \frac{\partial^2 Y_q(\eta)}{\partial \eta^2} d\eta \tag{A-19}$$

$$S_{rsgh}^{Ti} = \frac{EI_z}{2b_f^3} \sum_{r=1}^{M_2} \sum_{s=1}^{N_2} \sum_{g=1}^{M_2} \sum_{h=1}^{N_2} \int_0^1 Z_r(\xi) Z_g(\xi) \frac{\partial H_s(\eta)}{\partial \eta} \frac{\partial H_s(\eta)}{\partial \eta} d\eta \tag{A-20}$$

Notations

a	: length of the box girder
A	: areas of the ribs, respectively
b_f, b_w	: width of the flange and the web
E	: Young's modulus of the box girder
G	: shear modulus
I_y, I_x	: moment of inertia about the major and minor axes of the ribs
J	: torsional rigidity of longitudinal and transverse ribs, respectively
K^f, K^w	: buckling coefficients for the flange and the web, respectivel
N^f, N^{Li}, N^{Ti}	: applied forces on the flange and the ribs
$P_i(\xi)$, $\omega_j(\eta)$, $\Phi_m(\xi)$, $Y_n(\eta)$, $Z_r(\xi)$, $H_s(\eta)$	: displacement functions
Q	: first moment of inertia of longitudinal and transverse ribs, respectively
W^f, U^f, V^f	: flange displacement functions
sp^{Li}, sp^{Ti}	: ribs spacing in the longitudinal and transverse directions, respectively
t_f, t_w	: thicknesses of the flange and the web
Π^f, Π_{st}^{Li}, Π_{st}^{Ti}	: potential energy functions
b_{ij}, u_{mn}, v_{rs}	: amplitudes of the shape functions
$(\sigma^f)_{max}$	: buckling stress of the flange